Design and Fabrication of Force Sensing Robotic Foot Utilizing the Volumetric Displacement of a Hyperelastic Polymer

by

Matthew A. Estrada

Submitted to the Department of Mechanical Engineering
in partial fulfillment of the requirements for the degree of

Bachelor of Science in Mechanical Engineering

at the

MASSACHUSETTS INSTITUTE OF TECHNOLOGY

June 2012

ARCHIVES
MASSACHUSETTS INSTITUTE OF TECHNOLOGY
JUN 28 2012
LIBRARIES

© Massachusetts Institute of Technology 2012. All rights reserved.

Author .....
Department of Mechanical Engineering
May 10, 2012

Certified by .....
Sangbae Kim
Assistant Professor
Thesis Supervisor

Accepted by .....
John A. Lienhard V
Samuel C. Collins Professor of Mechanical Engineering

Design and Fabrication of Force Sensing Robotic Foot Utilizing the Volumetric Displacement of a Hyperelastic Polymer

by

Matthew A. Estrada

Submitted to the Department of Mechanical Engineering
on May 10, 2012, in partial fulfillment of the
requirements for the degree of
Bachelor of Science in Mechanical Engineering

Abstract

This thesis illustrates the fabrication and characterization of a footpad based on an original principle of volumetric displacement sensing. It is intended for use in detecting ground reaction forces in a running quadrupedal robot. The footpad is manufactured as a monolithic, composite structure composed of multi-graded polymers reinforced by glass fiber to increase durability and traction. The volumetric displacement sensing principle utilizes a hyperelastic gel-like pad with embedded magnets and Hall-effect sensors. Normal and shear forces can be detected as contact forces cause the gel-like pad to deform into rigid wells without the need to expose the sensor. A one-time training process using an artificial neural network was used to relate the normal and shear forces with the volumetric displacement sensor output. Two iterations on geometry are prototyped and tested. The first shows the ability to accurately predict normal forces in the Z-axis up to 80 N with a root mean squared error of 6% but little information about shear forces in the X an Y-axis. The second iteration demonstrates an ability to pick up the presence and direction of shear forces up to 40 N but with a root mean squared error of 70%. This project demonstrates a proof-of-concept for a more robust force sensor suitable for use in robotics that requires compliance while interacting with its environment.

Thesis Supervisor: Sangbae Kim
Title: Assistant Professor

Acknowledgments

I would like to thank Meng Yee (Michael) Chuah for his guidance and collaboration with this project, as well as birthing the idea for the sensor. I would also like to thank Sang Ok Seok for lending his expertise in LabVIEW and NI products when troubleshooting both hardware and software. Finally, I would thank Sangbae Kim and the rest of the Biomimetic Robotics Lab for the enjoyable years as a UROP and thesis student.

Contents

1 Introduction **11**

1.1 Design Considerations 11

1.1.1 Sensing Requirements 12

1.1.2 Functional Requirements of a Foot 13

1.2 Current Force Sensing Technology 13

1.2.1 Rigid Sensors 13

1.2.2 Compliant Sensors 14

1.2.3 Specialized Applications 14

2 Design and Fabrication **17**

2.1 Overview 17

2.2 Foot Design 17

2.2.1 Composite Monolithic Structure 19

2.2.2 Fabrication Process 19

2.3 Sensing Mechanism: Volumetric Displacement of an Hyperelastic Polymer . . 21

2.4 Force-Deformation Relation 23

2.4.1 Artificial Neural Network and Hall-effect Sensors 23

2.5 Two Iterations on Geometry 24

3 Experimental Results **27**

3.1 Experimental Procedure 27

3.2 Vertical Well Results 29

3.3 Angled Well Results 29

4 Discussion **33**

4.1 Clues from Raw Data 33

4.1.1 Volumetric Displacement vs. Displacement of Magnet Orientation . . 34

4.2 Conclusions 34

4.3 Future Work 36

4.3.1 Rigid Well Geometry 37

4.3.2 Linear Bearing 37

4.3.3 IR Sensing 37

4.3.4 Impact Testing 37

4.3.5 Reduction in Size 38

List of Figures

1-1 MIT Cheetah and Current Paw Design 12

2-1 Deformation of Elastomeric Padding within Foot Sensor 18
2-2 Assembled and Disassembled Footpad Force Sensor 20
2-3 Cross-sectional View of Fabrication Process 22
2-4 Two Iterations on Well Geometry 25

3-1 Experimental Setup with the CNC Milling Machine. 28
3-2 Two-Axis Shear Paths 28
3-3 Results for Vertically Oriented Well Geometry 30
3-4 Results for Angled Well Geometry 32

4-1 Raw Hall-effect Sensor Data vs. F/T Sensor 35

Chapter 1

Introduction

The thesis herein details the design, construction and initial characterization of a force-sensing foot intended for use in high-speed quadrupedal running on the robotic, MIT Cheetah, which is pictured in figure 1-1 along with its current, sensor-less footpad. The project continues in the same line as previous research on sensing in the footpad but seeks a higher level of integration [2]. The author's role focused on redesigning an existing footpad used with the robot to incorporate force sensing with limited change to the original design intent. The novelty of the project lies in the exploration of a new mechanism of "volumetric displacement" of a hyper-elastic polymer to sense force, which allows the developed end effector to perform well as both a sensor and foot. No off-the-self sensors found could incorporate compliance, sense shear loads, or sense a high range of forces while exhibiting light weight and low "inertial noise" when accelerated at high speeds.

1.1 Design Considerations

High speed running places great demands on the capabilities of any robot hoping to achieve successful locomotion. The challenge in designing a robotic foot for this highly dynamic application is twofold; the ability to measure ground reaction forces is arguably the most inportant sensor on the robot and the dynamics of foot-ground contact is critical since it is the only interface in which the robot actually interacts with its environment. Both these sets of distinct requirements must be fulfilled.

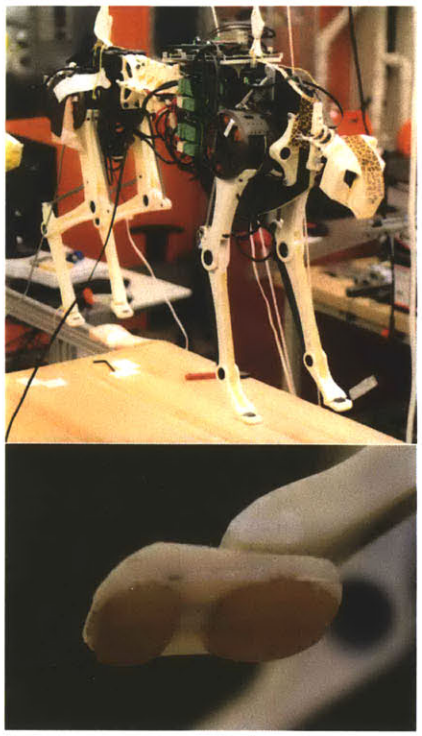

Figure 1-1: MIT Cheetah and Current Paw Design

1.1.1 Sensing Requirements

In order to provide useful feedback and control, the ground contact model perceived by the robot should be as accurate as possible. In running, this necessitates force sensing to have a high range in both normal and shear directions for a complete picture of ground reaction forces. The cheetah can take up to three times its body weight on a foot while running, translating to a peak force of 1000 N on any given foot. Additionally, the act of running itself entails repeated impacts rather than sustained forces, so the bandwidth of the sensor must be able to handle this time scale. Finally, detecting touchdown of the foot is also of utmost importance in controlling locomotion.

In a previous test of a single leg, the hardware was accelerated to a horizontal velocity of 2.6 m/s and allowed to take a single bound onto a force plate. The peak normal force recorded was 550 N, and the peak shear force was 100 N. Both force profiles took place over a period of 180 ms in which the foot was in contact with the ground.

1.1.2 Functional Requirements of a Foot

As the sole interface between the robot and the ground, the foot is the only means with which a legged machine can generate reaction forces with its environment. The ability to adapt to asperities in the ground, absorb impacts, provide traction, and store and release energy are all important functions [4, 5]. Indeed, it has been shown that the viscoelastic properties of mammalian paw pads are critical in ensuring a desirable dynamic response under impacts such as those experienced during running [1]. Additionally, the foot must be tough enough to withstand the impact of repeated foot strikes during running, so durability is a central issue as well.

This diversity of goals in an ideal foot presents a sensing problem that occupies a niche not readily addressed by off-the-shelf solutions.

1.2 Current Force Sensing Technology

Though tactile sensing has been the focus of much research within the field of robotics, current sensing methodologies are almost invariably designed separately from the robot itself, often utilizing standard components. This results in sensors that are added-on to the robot instead of being fully incorporated into the robot's design, which can be problematic for a number of reasons.

1.2.1 Rigid Sensors

The most conventional of approaches to force sensing fail to incorporate the compliance that is essential for successful interaction with terrain while running [1]. These methods have often taken a policy of separating a robot from its environment by placing the sensor directly between robot and ground. Reaction forces acting upon the machine are often rerouted and transmitted through the sensor to attain a measurement which ultimately alters the original mechanics. The gold standard, a traditional force/torque (F/T) sensor, is one example of such a methodology that is commonly found in industrial robotics and humanoid robots used for research. 'KH-R3' Hubo [11] and 'LOLA' [7] are two examples of humanoid robots that use a custom F/T sensor in each foot for sensing ground contact. The direct use of F/T sensors for force sensing in the foot makes the foot much more bulky and weighs the robot down. 'BIPMAN' attempts to emulate the human foot, but still uses multiple off-the-shelf

sensing solutions [5].

Furthermore, the broader approach of measuring the deformation of rigid structures, as is done in F/T sensors, is less than ideal despite the allure of linearity and repeatability in measurements. Such a method would require the need for sensors to be mounted far from the foot-ground contact, either with compliant mechanisms between the two or depend on a rigid contact surface with the ground that would likely result in chatter [1].

1.2.2 Compliant Sensors

Compliant sensors take a different approach but often encompass many concerns significantly removed from those required in the demands of running. Scalability, adaptability to curved surfaces, low power consumption, and cost all aim to maximize the sensors' utility in a wide range of applications as a "artificial skin" [15, 6]. Likewise, tactile sensors for human gait analysis within medical studies seek to fill a similar niche but are constrained by the need to interface with existing footwear and measure many more parameters than are required for robotic running. As a result, the subsequent design integrates many different types of sensors and supporting hardware irrelevant to simply measuring ground reaction force and touchdown [9]. While this and other similar solutions are well suited for retroactively fitting robots with the ability to sense touch or comprehensively measuring physiological parameters, there is still much to be desired when considering the dynamic requirements of the footpad on a running quadruped. It is desirable to extract only the essential measurements and minimize the demand put on the control system, which must compute in real-time during running.

1.2.3 Specialized Applications

Given the aforementioned challenges in matching off-the-shelf sensors to a very specialized application, designing the sensing solution in tandem with the robot can result in great advantages. For example, the musculoskeletal humanoid 'Kojiro' innovatively utilizes joint-angle sensors found in mobile phones in its spherical joints [16]. Another example of this is seen in the custom-built strain sensor developed by Park et al. for use in their active soft orthotic device [12]. Similarly, the exoskeletal end effectors embedded with optical fiber Bragg grating sensors Park et al. are another example of a robot's structure and sensing being designed in tandem [13].

It is proposed here for the fabrication of a novel integrated force sensor with applications in a running robotic quadruped. Due to the current limitations in sensing technologies, there is a need for a light-weight, resilient force sensor for use in a running quadrupedal robot, which the footpad in this paper seeks to fill.

Chapter 2

Design and Fabrication

2.1 Overview

The integrated, volumetric displacement force sensor presented in this section utilizes the novel approach of sensing the deformation of a soft, elastomeric padding into an array of rigid wells, as depicted in figure 2-1. Small magnets are mounted onto the padding, which allows the proximity of the elastomer's surface to be sensed by Hall-effect sensors placed above these wells. As the wells are part of a single elastomer, any shear on the foot will affect the individual wells and magnets differently. This results in a change in the Magnetic Flux Density (MFD), which is then recorded via the Hall-effect sensors. Using an artificial neural network to calibrate the system once, the MFD is related to the measured normal and shear forces. A photo of the monolithic foot structure, the rigid well insert, and Hall-effect sensors mounted onto a printed circuit board (PCB) are shown assembled and disassembled in figure 2-2, along with the cross-section of a completely monolithic iteration. Two iterations on the geometry of the rigid wells were investigated, as shown in figure 2-4.

2.2 Foot Design

The concept behind the current footpad design has gone through multiple design iterations and demonstrated robust performance with the MIT Cheetah, as pictured in figure 1-1. The biomimetic design was inspired by the texture and shape of feline paws, particularly the ability to offer compliance under normal forces while offering a resistance to strain under shear forces.

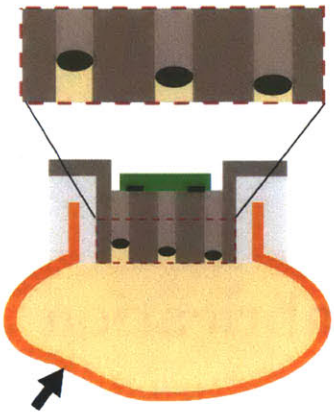

Figure 2-1: Deformation of Elastomeric Padding within Foot Sensor

Firstly the tougher, outer "skin" of the foot was cast using a durable rubber, Vytaflex® 20, in order to withstand the wear that repeated impact and loading would impose on the material. The rubber material also provides a high coefficient of friction to generate sufficient forces tangent to the ground during contact.

The anisotropic compliance acts as a mechanical, low pass filter, conforming to small asperities in the ground while leveling on the larger gradient of the terrain. Additionally, woven glass fiber embedded within the "skin" ensures that the foot maintains structural integrity under shear. This combination allows the foot to increase the surface area with which it contacts the ground to increase traction and couples it with the ability to transmit these shear forces through to the leg and the body. Additionally, anisotropic compliance further facilitates the driving mechanism utilized by the sensor, as the soft elastomer is prevented from slipping out from under the foot due to shear, but uninhibited from being pushed up inside the rigid wells when loaded under normal forces.

The footpad featured in this paper is a prototype in which to test the sensing mechanism described in latter sections and was enlarged for ease of assembly and iteration on designs. Final footpad designs will be significantly smaller.

2.2.1 Composite Monolithic Structure

The sensor was fabricated by casting several different thermosetting polymers to one another. The monolithic design was chosen to promote robustness during impact and minimize the size the sensing unit occupied. As an added benefit, since the sensor is completely encased in the footpad, it is protected from the environment and unlikely to fail. An illustrated overview of the process can be seen in figure 2-3.

An assembled, disassembled, and cross-sectional view of the footpad sensor is depicted and labeled in figure 2-2. Labeled components are (A) the outer "skin" of woven fiberglass embedded in polyurethane rubber, (B) the soft silicone rubber to form "padding" inside "skin," (C) the outer plastic for mounting and structure, (D) the magnets mounted on top of silicone rubber, (E) the ABS rigid well insert and (F) the array of four Hall-effect sensors. In the bottom, cross-sectional view, a completely monolithic prototype was used, casting the outer wall and rigid wells (C & E) as a single piece of Task® 4 plastic.

The final weight of the full prototype with ABS insert was 95 grams, while completely monolithic iterations weighed only 60 grams once the wells were cast directly out of Task® 4 plastic. Final designs would likely be close to half this weight after the size had been reduced. The mechanism of measuring the volumetric displacement of a polymer within the footpad also means that the amount of mass available to give rise to undesirable dynamic effects is minimal. Traditional F/T sensors, when rapidly accelerated, show phantom forces that are not being applied to the interface intended to be measured. This is presumably due the force being transmitted through the sensing mechanism in order to accelerate any mass in series with it. In the current design, only 35g of mass is present between the sensor and the ground. The mass itself is a visco-elastic material and offers its own damping to dissipate oscillations. During tests compared directly with a Force/Torque sensor, the footpad sensor faired much better.

2.2.2 Fabrication Process

Several polymers were cast on top one another during the fabrication process. Figure 2-3 depicts the lettered steps in molding the composite footpad detailed in this section. First, the tough, outer "skin" of the foot was constructed by wrapping woven fiberglass around a shaped insert (decpicted in step A) and pressing it into a mold (B), embedding it within

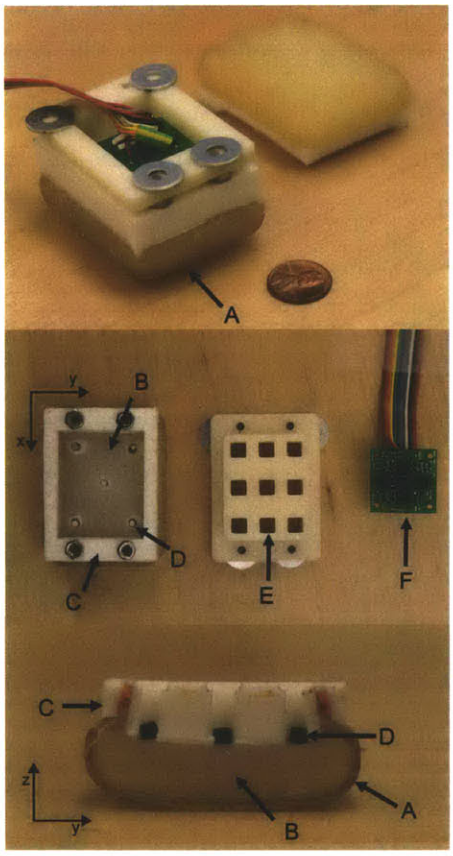

Figure 2-2: Assembled and Disassembled Footpad Force Sensor

a 2mm thick layer of Vytaflex ® 20 polyurethane rubber of shore hardness 20A. After demolding, the skin retained the shape imposed by the casting process and was flexible enough to peel off the internal, shaped insert. Next, the urethane "skin" was filled with Ecoflex ® Supersoft Silicone rubber of a very soft shore hardness, 00-10A, which was allowed to self-level (C & D).

A rigid, outer lining was cast on top of these rubbers (E & F) using Task® 4 polyurethane resin of shore hardness 83D. The rigid lining provided structural integrity and allowed for a separate, ABS insert to be anchored onto the foot which imposed the rigid wells above the silicone rubber (G & H). The use of a separate, ABS insert allowed for rapid iteration on the geometry of the wells, and greater ease in securing the magnets to the top of the silicone rubber. This was done with cyanoacrylate. Ultimately, the ABS insert would be replaced by casting well geometry directly into the Task ® 4 once an optimal configuration had be conferred upon.

2.3 Sensing Mechanism: Volumetric Displacement of an Hyperelastic Polymer

In order to measure force, it must be converted into a quantity that can readily be measured as a signal. The deformation of the soft elastomer within the paw pad was chosen as the sensing mechanism. The illustration in figure 2-1 depicts this principle operating within the footpad. As ground reaction forces are applied to the footpad in this cross-sectional view, the soft elastomer deforms up into the rigid wells, sending a unique signal, based on the normal and shear components, to the Hall-effect sensors mounted above.

Implementing this sensing mechanism required no additional mass to the foot but rather hollowing out wells in the rigid, plastic structure of the top of the foot while inserting small magnets and Hall-effect sensors into the structure. The chosen mechanism incorporates the compliance necessary to facilitate successful interaction with terrain, minimizes need for additional weight or components, and allows for a monolithic and robust structure.

Additionally, the presented mechanism strives to attain a greater level of sensor integration within a compliant structure. By being completely integrated into the foot, it preserves the original design intent, promotes dynamics favorable to running, and measures ground reaction forces as close to the foot-ground interface as possible.

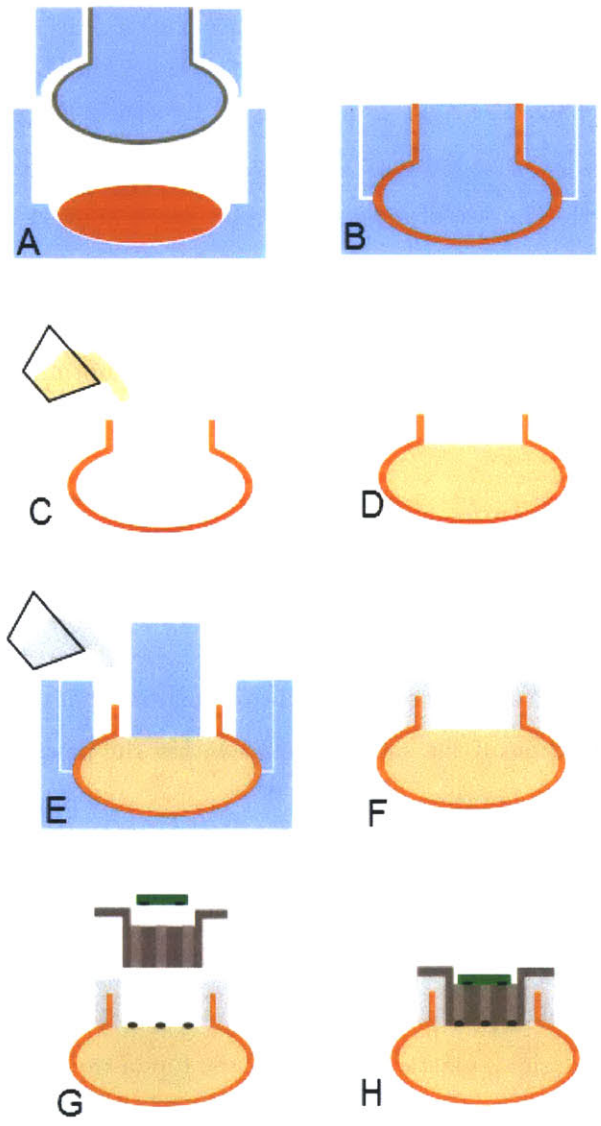

Figure 2-3: Cross-sectional View of Fabrication Process

2.4 Force-Deformation Relation

Attaining an analytical relation between the change in magnetic flux density read by the sensors and the forces causing the deformation of the footpad is non-trivial. Two highly non-linear equations must be solved in order to map both the deformation of the elastomer and the subsequent change in magnetic flux density. Models for hyper-elastic materials such as those presented by Mooney-Rivlin [14], Arruda-Boyce [3] and Ogden [10] prove to be highly dependent on the quality of the experimental data collected for the given material. Additionally, the geometry presents an overly complicated situation comprising of two separate elastomers deforming in series. One of the polymers is embedded with an anisotropic, woven material while the other is pressing up into a rigid structure. This makes it very difficult to predict the change in height and orientation of the magnets in the wells.

Additionally, simulating the physical situation with finite-element analysis was explored but the situation still proved to be overly complex, taking an unreasonable amount of time to solve for a given set of initial conditions and still relying on hyper-elastic material models.

Hence, it was decided to map the output of the Hall-effect sensors to the input of the ground reaction forces that produced it through the use of an artificial neural network (ANN).

2.4.1 Artificial Neural Network and Hall-effect Sensors

An atrificial neural network is a computational model used to correlate an input and an output signal or find patterns in data. The form is inspired by biological neural networks and is an adaptive system consisting of nodes that change their structure and strength of connections based on an iterative training procedure utilizing previously collected data.

In this specific case, the change in the MFD is parsed and empirically correlated to the applied forces using the Neural Network Toolbox within Matlab. A feed-forward neural network is created where an input-output relationship is mapped between the MFD as measured by the 4 Hall-effect sensors and the forces recorded by a F/T sensor. The Levenberg-Marquardt optimization network training function [8] then uses a back-propagation algorithm to update the weights and bias values of the neural network until the minimum mean squared error is obtained and the desired performance is realized. The Levenberg-Marquardt algorithm is given as:

$$[J^T W J + \lambda diag(J^T W J)]\delta = J^T W[F(t) - \hat{F}(t)] \tag{2.1}$$

where J is the gradient matrix, W is the weighting matrix, λ is the algorithmic parameter, δ is the increment in each iteration, F(t) is the target force output from the F/T sensor and F(t) denotes the force estimates of the ANN. This work on the use of artificial neural networks for force sensing is further elaborated on in the paper by Ananthanarayanan et al. [2].

The specific Hall-effect sensors used in this prototype was a set of four, Sentron CSA-1VG sensors. The linear, 1-Axis Hall-IC sensors are sold for a unit price of about $5 for small quantities.

2.5 Two Iterations on Geometry

Two configurations were prototyped varying the geometry of the rigid wells into which the magnets pressed into, which only required 3D printing a new ABS insert and connecting new sensors. The laborious process of molding the a new footpad was avoided, and the same physical footpad was used.

The first iteration consisted of nine, vertically-oriented wells, of which five were embedded with magnets facing upwards, their poles all aligned parallel. Magnets were placed in the wells at the outer corners and one in the center well. In this instance, the Hall-effect sensors were placed in a cluster around the center of the pad, as pictured in figure 2-2.

The second iteration consisted of four, angled wells pointing towards the corners of the footpad and was motivated by a desire to increase the accuracy with which the sensor could pick up shear forces. In this configuration, a Hall-effect sensor was placed to align it's sensitive axis with the center axis of the well, and an attempt was made to align the pole of the magnet with this same axis.

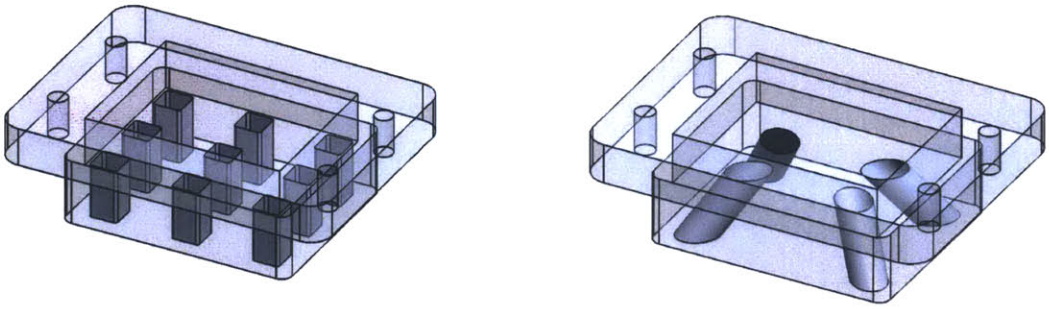

Figure 2-4: Two Iterations on Well Geometry

Chapter 3

Experimental Results

The experimental verification of the footpad sensor centered on evaluating the sensor's accuracy at reading normal and shear reaction forces under position control at the speed of 200mm/s.

3.1 Experimental Procedure

In order to get training data to feed into the neural network, the foot was precisely moved to fixed displacements while the reaction forces were recorded. This was achieved by mounting the footpad to an industrial 3 axis CNC milling machine (HAAS Super Mini Mill 2). The footpad was attached directly to the quill and a separate mount for attaching the F/T sensor to the mill table. This experimental setup is shown in figure 3-1.

The training data was generated by displacing the footpad sensor into the F/T sensor a fixed depth, then moving it in-plane along a two-axes path, as shown within figure 3-2, submitted it to shear forces along the X and Y-axis. The footpad was displace at increments between 1mm and 3mm into the F/T sensor to generate a normal load. After each vertical displacement, the shear path traversed the footpad 5mm in both the positive and negative directions along the X-axis. This was then repeated in the Y-axis. Finally, the footpad was made to follow a circular path of 10mm diameter about the origin.

For verification, more data was gathered with an arbitrary path. This path involved a diagonal motion of 5mm in each of the 4 quadrants of the X and Y-axis. This was then followed with 4 smaller circular paths of 5mm diameter along each of the positive and negative X and Y-axis.

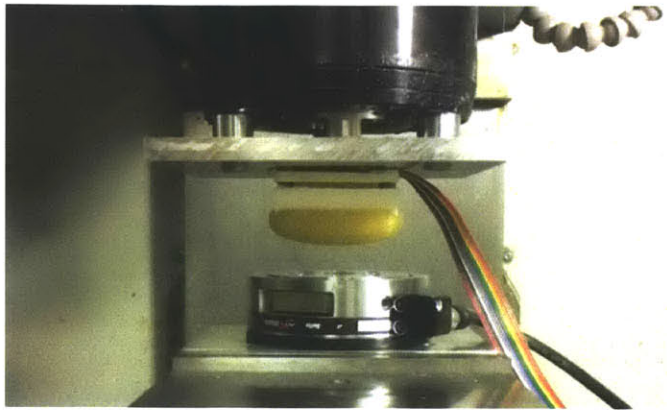

Figure 3-1: Experimental Setup with the CNC Milling Machine.

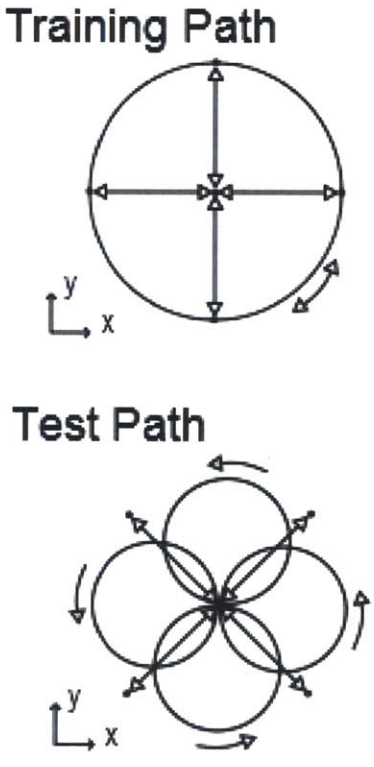

Figure 3-2: Two-Axis Shear Paths

3.2 Vertical Well Results

The results for the footpad sensor with wells oriented in a vertical geometry showed accurate results with forces oriented in the Z axis, though readings on shear forces were lacking. The plots for the force readings, after correlation through the artificial neural network, are shown in figure 3-3, as compared against the measurements taken from the F/T sensor.

Results showed that the neural network is able to predict normal forces in the Z-axis up to 80N with great accuracy. The root mean squared (RMS) error was 4.83 N, which translated to 6.04% of the mean force being measured. This is followed by the Y-axis where shear forces of 40N are detectable, but the predicted force magnitudes are very inaccurate. The RMS error in this case is 12.90 N. In the X-axis, similar performance is observed where the RMS error for the X-axis is 16.76 N. It is important to note that the qualitative performance of the shear axes is also very inaccurate; the data often shows ANN predicted measurements that is positive or negative in value when the actual value is of opposite sign, which would be very problematic in controlling the robot.

Note that the noise levels in these graphs is due to electromagnetic interference (EMI) from the CNC milling mchine, and would inevitably improve in environments more natural to running. A Butterworth filter with a 10Hz cutoff frequency was applied to the gathered signals to remove the EMI noise.

Due to the inaccurate results with measurements of shear forces, a second iteration on the geometry of the rigid wells was constructed and tested.

3.3 Angled Well Results

The results from magnets pushing up into angled, rigid wells showed an improvement in the ability to pick up shear experienced in one axis, at the cost of accuracy in the Z axis. The respective plots for the results are shown in 3-4.

The improvement in the ability to pick up shear can easily be seen in the plot for results in the X axis. A RMS error was 11.28 N was present. While this corresponds to an error of 70% of the mean measured magnitude of 15.99 N, a significant improvement is seen in the qualitative aspects of the data. The ANN predicted measurements closely follow the sign of the actual reaction forces, though the magnitudes at peak forces tend to fall short of actual values. Unfortunately, the RMS error was 21.96 N in the Y axis, and 18.54 N in the

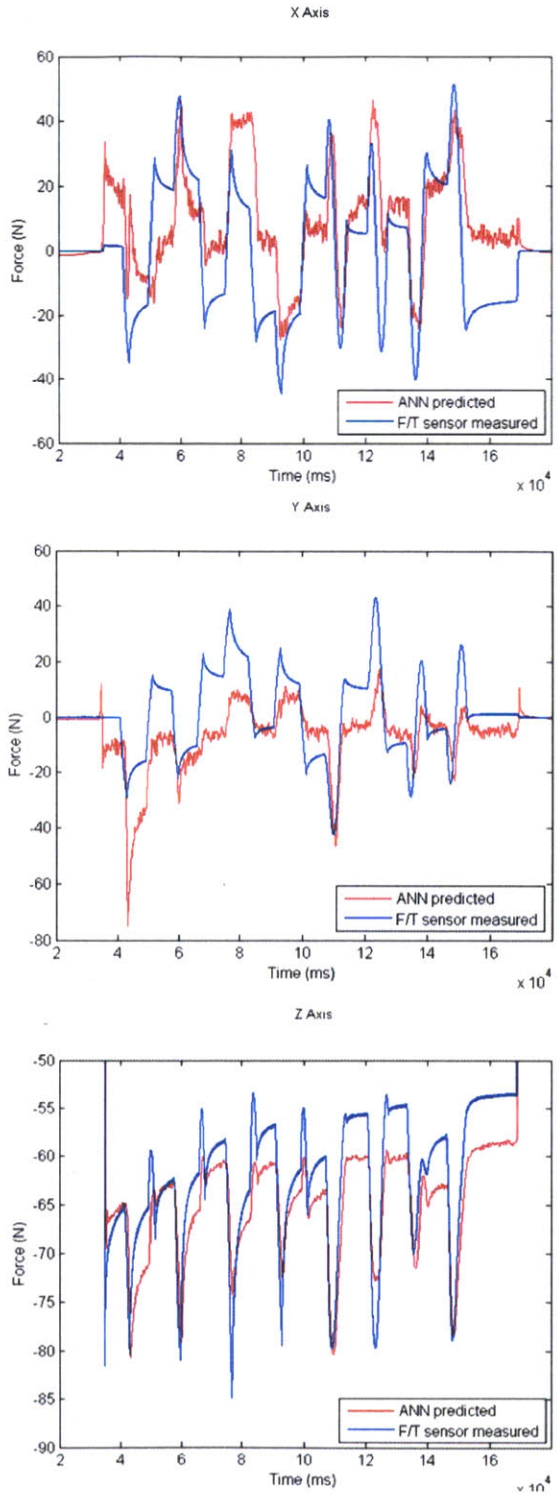

Figure 3-3: Results for Vertically Oriented Well Geometry

Z axis. Overall, this configuration seemed to perform worse, though it acts as a proof-of-concept that it is indeed possible to pick up shear with the sensor reliably in a qualitative and approximately in a quantitative sense.

Further inspection of the raw data for this experiment lends insight to the workings behind the accuracy of each signal.

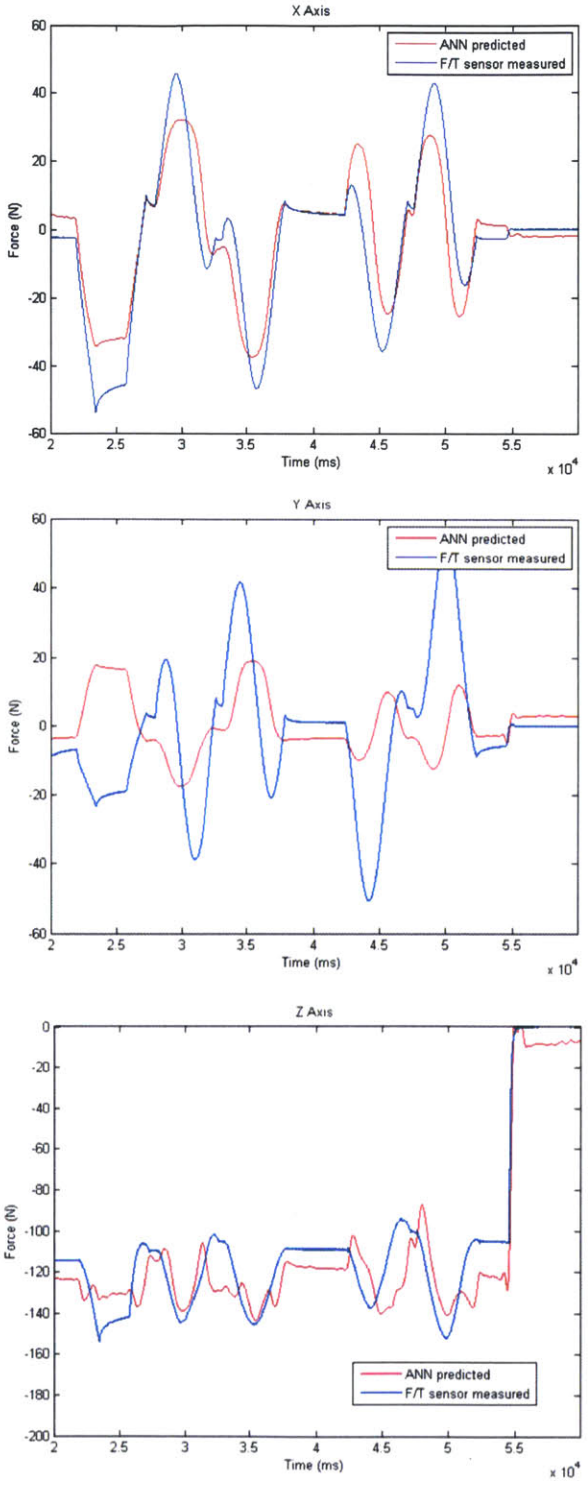

Figure 3-4: Results for Angled Well Geometry

Chapter 4

Discussion

4.1 Clues from Raw Data

Insight can be drawn from a close comparison of the uncorrelated signal received from the sensors and the forces recorded from the F/T sensor. Figure 4-1 shows the same Hall-effect data that was used to produce the results in figure 3-4 before it was parsed through the artificial neural network. Note that the Hall-effect sensor output was still passed through a low pass filter to remove the noise caused by EMI from the CNC mill and the output from sensor 1 contained a consistent offset throughout all the data. This data was taken from the angled well geometry.

All four sets of magnets and sensors were designed symmetrically and wired identically, however, discrepancies arise between their output signals. It can be seen that sensor 1 is particularly sensitive to shear forces along the X-axis. Similarly, sensor 2 follows the rise and fall of forces in the Z-axis, despite missing the initial peak when the footpad first makes contact. Unfortunately, the other two sensors fail to pick up meaningful measurements from any axes. It is also important to consider that none of the angled wells were aligned with a principle axis, but skewed to be pointed towards the four corners of the footpad.

While it is unclear why certain sensors performed much better than others, it is likely to be due to the complex relationship between the Hall-effect sensor output, and the actual displacement of the magnet due to ground reaction forces. A large part of this uncertainty should be due to the process of securing the magnets to the surface of the elastomeric padding. This was especially difficult when required to place the magnets at an angle intended to match the center axis of the rigid well. The process was done by hand and

noticeable discrepancies were seen in both the angle and exact position the magnet was mounted on the elastomer.

4.1.1 Volumetric Displacement vs. Displacement of Magnet Orientation

The author's intuition points towards and idealization made in figure 2-1, when the concept of measuring "volumetric displacement" was introduced. Rather than truely measuring the volumetric displacement of the elastomer into the rigid well, the Hall-effect sensor measures the change in MFD resulting from the displacement of the magnet attached to the surface of the elastomer. Figure 2-1 depicts the magnets rising straight up into the rigid wells. However, as the elastomer deforms, it can be observed that the magnet not only rises but changes orientation in pitch and roll angles, also augmenting the MFD. The Hall-effect measurements did not only pick up the bulging of the elastomer into the well, but the gradient of elastomer's surface which in turn determined the magnet's orientation that was rigidly fixed to it.

Just as important, the magnet's initial position and orientation likely had a large part in determining the strength of the signal from the sensor. This would be have affected the alignment of the magnet's pole, again affecting the MFD. Just as likely, the actual path through which the magnet traveled into the rigid well was not ideal in the angled case. In some loadings a magnet would contact the side of the well, doubtlessly affecting the measurement.

While on the subject of subtleties of utilizing magnets, it is worth noting that using magnets in conjunction with Hall-effect sensors does not allow for completely isolated measurements of the displacement from each rigid well–the magnetic field of each magnet affects all sensors to an extent. However, since the strength of the MFD falls off as the square of distance, sufficient spacing between magnets and sensor pairs can solve this problem.

4.2 Conclusions

This paper presents a proof-of-concept, dual-purpose footpad with integrated force sensing capabilities. A novel mechanism to remedy designing for the two distinct sets of considerations for sensors and footpads is presented and the feasibility to measure both normal and shear forces is demonstrated.

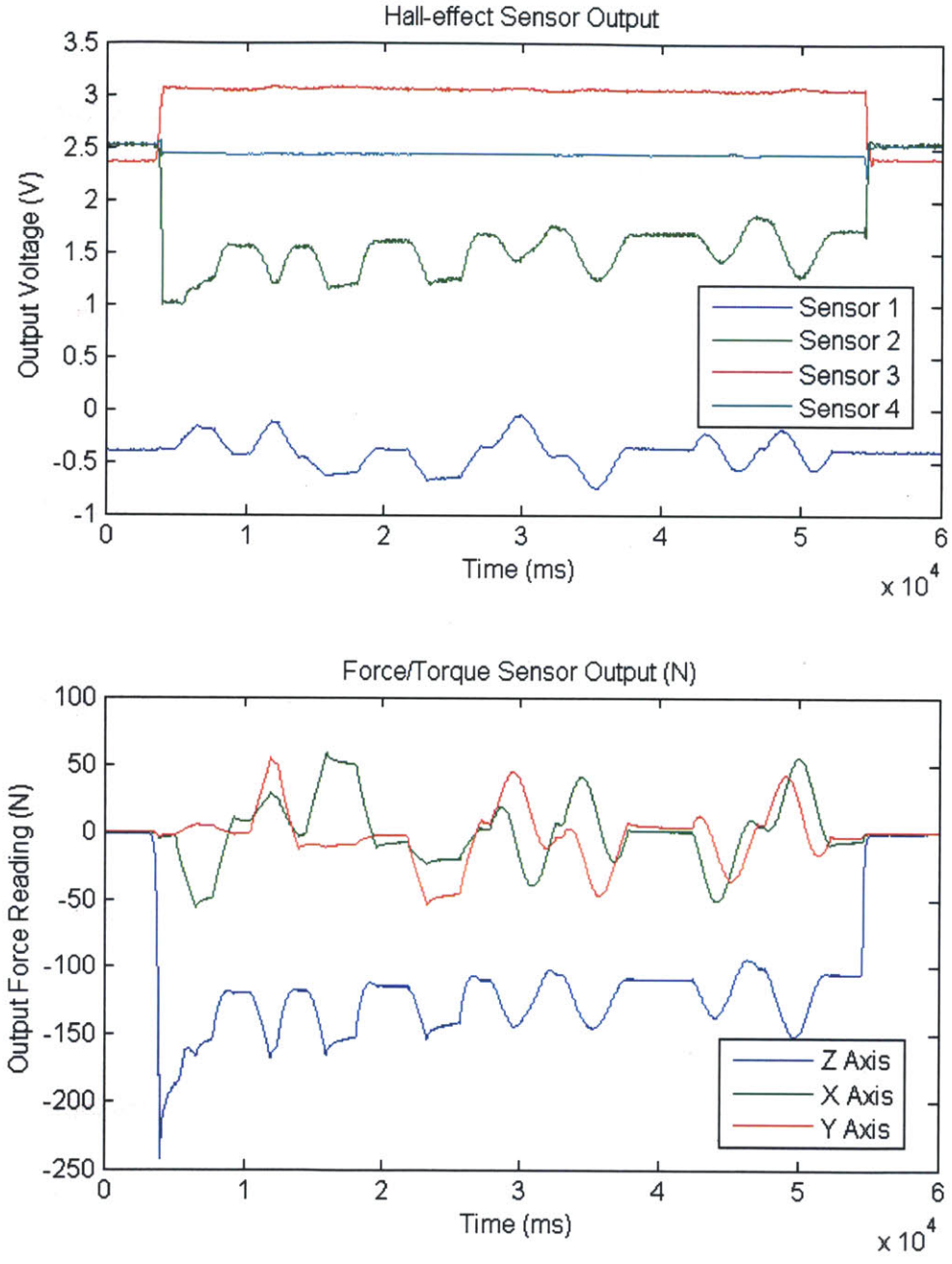

Figure 4-1: Raw Hall-effect Sensor Data vs. F/T Sensor

In summary, the design of the footpad makes use of the strengths of 3 different polymers to produce a footpad that is durable under repeated ground impacts while still being compliant enough to offer good traction. The volumetric displacement sensing principle utilizes a hyperelastic gel-like pad with embedded magnets, which allows normal and shear forces to be detected indirectly without the need to expose the sensor. A one-time training process using an artificial neural network is all that is necessary to relate the normal and shear forces with the volumetric displacement sensor output. The volumetric displacement sensor is able to detect normal forces up to 80N with a RMS error of 6.04% and the onset of shear forces in both the X and Y axis. This is a robust footpad sensor suitable for use in all outdoor conditions. This footpad is intended for use in the MIT Robotic Cheetah to detect whether ground contact and shear has occurred.

Applications for this force sensor span widely across any situation that requires force feedback for a robot interacting with its environment where it is preferable to have a compliant hand, rather than a rigid metal end effector. Furthermore, with all operating mechanisms fully encapsulated within the footpad, sensing is robust to outside disturbances and feasible to applications within hazardous environments. The developed footpad sets itself apart from currently available force sensing technology due to it's high range in forces able to be sensed, it's robustness to undesirable dynamic effects under high acceleration, and its integrated compliance in conjunction with its ability to pick up shear force measurements.

4.3 Future Work

Future work should first and foremost focus on refining the repeatability of the mechanism through which the deformation of the elastomeric pad is measured. At the very least, this would consist of a more standardized procedure to attach the magnets to the top of the elastomer. Molding recesses to cup the magnets into a particular orientation, or constructing a magnetic stage to reliably align the orientation of the small magnet's poles would also increase repeatability. Furthermore, several more in-depth improvements can bring the sensor closer to being used on the MIT Cheetah.

4.3.1 Rigid Well Geometry

The results shown in discussion suggest that a single well with a single magnet may be sufficient to measure a principle axis reliably. Some sensors followed force profiles fairly accurately. Indeed, to combine the best of both iterations, the logical next step would incorporate both vertically oriented and angled wells, the latter of which may benefit from being aligned with the X or Y-axis.

4.3.2 Linear Bearing

To reliably fix the initial position of the magnet, as well as its path through the rigid well, a linear bearing would be ideal. Constraining the degree of freedom to a single, desired path would greatly increase the reliability of measurements. One possible solution may be to mount the magnet in a loose, sliding fit within teflon tubing rather than having a the magnet loosely push up up into a hole much larger than itself.

4.3.3 IR Sensing

One currently unexplored option is to incorporate IR sensing rather than Hall-effect sensors. IR would decouple the sensors from one another since no magnetic fields would overlap. This would require a dark coating on the soft elastomer's surface to ensure no ambient light would leak into the reading. This solution, however, may still be subject to the gradient of the elastomer's surface in the well, since it would affect the reflection of light.

4.3.4 Impact Testing

To verify that this sensor will be useful in sensing impacts similar to running, proper evaluation would entail impact testing. Such testing would more fully characterize the aspects of impacts that the sensor measured accurately, such as peak force, the envelope of the force profile, or the overall change in momentum. Additionally, the effects that the visco-elastic polymer had on the ability to sense time-sensitive force measurements may be of interest. Correlating a set of forces that shared a more uniform form, such as that of an impact, may also improve the results of the ANN.

4.3.5 Reduction in Size

Before actual implementation with the MIT Cheetah, the final design of the sensor would entail scaling down the size of the footpad to reduce the weight which the cheetah must swing with its leg. This would become possible once the geometry of the rigid wells, size of magnets, and orientation of sensors were optimized and conferred upon.

Bibliography

[1] R. McN. Alexander, M. B. Bennett, and R. F. Ker. Mechanical properties and function of the paw pads of some mammals. *Journal of Zoology*, 209(3):405–419, July 1986.

[2] A. Ananthanarayanan, S. Foong, and S. Kim. A compact two dof magneto-elastomeric force sensor for a running quadruped. *International Conference on Intelligent Robots and Systems, to appear*, 2012.

[3] Ellen M. Arruda and Mary C. Boyce. A three-dimensional constitutive model for the large stretch behavior of rubber elastic materials. *Journal of the Mechanics and Physics of Solids*, 41(2):389–412, February 1993.

[4] S Davis. The design of an anthropomorphic dexterous humanoid foot. *and Systems (IROS), 2010 IEEE/RSJ*, pages 2200–2205, 2010.

[5] M. Guihard and P. Gorce. Biorobotic foot model applied to BIPMAN robot. *2004 IEEE International Conference on Systems, Man and Cybernetics (IEEE Cat. No.04CH37583)*, 7:6491–6496, 2004.

[6] T. Hoshi and H. Shinoda. Robot skin based on touch-area-sensitive tactile element. In *Proceedings 2006 IEEE International Conference on Robotics and Automation, 2006. ICRA 2006.*, pages 3463–3468. IEEE.

[7] S. Lohmeier, T. Buschmann, and H. Ulbrich. System design and control of anthropomorphic walking robot lola. *Mechatronics, IEEE/ASME Transactions on*, 14(6):658–666, 2009.

[8] DW Marquardt. An algorithm for least-squares estimation of nonlinear parameters. *Journal of the society for Industrial and Applied ...*, 1963.

[9] Stacy Morris. *A shoe-integrated sensor system for wireless gait analysis and real-time therapeutic feedback.* 2004.

[10] R. W. Ogden. Large Deformation Isotropic Elasticity - On the Correlation of Theory and Experiment for Incompressible Rubberlike Solids. *Proceedings of the Royal Society A: Mathematical, Physical and Engineering Sciences*, 326(1567):565–584, February 1972.

[11] Ill-woo Park, Jung-yup Kim, Jungho Lee, and Jun-ho Oh. Mechanical design of humanoid robot platform KHR-3 (KAIST humanoid robot - 3: HUBO). *5th IEEE-RAS International Conference on Humanoid Robots, 2005.*, 3:321–326, 2005.

[12] Y.L. Park, B. Chen, D. Young, L. Stirling, R.J. Wood, E. Goldfield, and R. Nagpal. Bio-inspired active soft orthotic device for ankle foot pathologies. In *Intelligent Robots and Systems (IROS), 2011 IEEE/RSJ International Conference on*, pages 4488–4495. IEEE, 2011.

[13] Y.L. Park, S.C. Ryu, R.J. Black, K.K. Chau, B. Moslehi, and M.R. Cutkosky. Exoskeletal force-sensing end-effectors with embedded optical fiber-bragg-grating sensors. *Robotics, IEEE Transactions on*, 25(6):1319–1331, 2009.

[14] R. S. Rivlin. Large Elastic Deformations of Isotropic Materials. IV. Further Developments of the General Theory. *Philosophical Transactions of the Royal Society A: Mathematical, Physical and Engineering Sciences*, 241(835):379–397, October 1948.

[15] J. Ulmen and M. Cutkosky. A robust, low-cost and low-noise artificial skin for human-friendly robots. In *Robotics and Automation (ICRA), 2010 IEEE International Conference on*, pages 4836–4841. IEEE, 2010.

[16] J. Urata, Y. Nakanishi, A. Miyadera, I. Mizuuchi, T. Yoshikai, and M. Inaba. A three-dimensional angle sensor for a spherical joint using a micro camera. In *Proceedings of the 2006 IEEE International Conference on Robotics and Automation*, pages 82–87, 2006.